Microscopic investigation of the Johari-Goldstein relaxation in cumene

Insights on the mosaic structure in a van der Waals liquid

Caporaletti, F.; Capaccioli, S.; Bessas, D.; Chumakov, A.I.; Martinelli, A.; Monaco, G.

Link to publication

Microscopic investigation of the Johari-Goldstein relaxation in cumene: Insights on the mosaic structure in a van der Waals liquid

Federico Caporaletti [a,b,*,1], Simone Capaccioli [c,d], Dimitrios Bessas [e], Aleksander I. Chumakov [e], Alessandro Martinelli [f], Giulio Monaco [f,*]

[a] Van der Waals-Zeeman Institute, Institute of Physics, University of Amsterdam, Science Park 904, Amsterdam, 1098XH, the Netherlands
[b] Van 't Hoff Institute for Molecular Sciences, University of Amsterdam, Science Park 904, Amsterdam, 1098XH, the Netherlands
[c] Dipartimento di Fisica, Università di Pisa, Largo Bruno Pontecorvo 3, Pisa, I-56127, Italy
[d] CISUP, Centro per l'Integrazione della Strumentazione dell'Università di Pisa, Lungarno Pacinotti 43, Pisa, I-56127, Italy
[e] ESRF-The European Synchrotron, CS40 220, Grenoble Cedex 9, 38043, France
[f] Dipartimento di Fisica ed Astronomia, Università di Padova, Via F. Marzolo, 8, Padova, I-35121, Italy

ARTICLE INFO

ABSTRACT

The Johari-Goldstein (β_{JG}) relaxation anticipates in time, and is closely connected to, the structural relaxation in deeply supercooled liquids. Probing its microscopic properties is a crucial step for a complete understanding of the glass-transition. We here report the investigation of the van der Waals glass-former cumene using time-domain interferometry, a technique able to probe microscopic density fluctuations at the spatial and temporal scales relevant for the β_{JG}-relaxation. We find that the molecules participating in it undergo a restricted motion, though sufficient to induce local, cage-breaking events at the characteristic time-scale for molecular re-orientations. A detailed characterization of the relaxation strength, i.e. the fraction of molecules involved in the relaxation process, shows that such molecules are connected in a percolating cluster which, above the glass-transition temperature, T_g, is weakly dependent on temperature. Our results confirm thus previous observations of a mosaic structure associated to the β_{JG}-relaxation in the supercooled state, and provide additional information on its temperature evolution above the glass-transition temperature. We conclude that the observed microscopic properties of the β_{JG}-relaxation, and thus of the associated mosaic structure, are generic and independent of the molecular interaction potential. In addition, we show that, while the dynamics within the percolating cluster becomes progressively slower on approaching T_g, the fraction of the molecules involved in cage-breaking events within the β_{JG}-relaxation is not affected by temperature.

1. Introduction

The microscopic origin of the glass-transition is a long-standing question which remains incompletely solved despite the collective effort of several generations of scientists. On approaching the glass-transition temperature (T_g) the dynamics of supercooled liquids dramatically slows down. This increase in the characteristic timescale for microscopic motion is accompanied by anomalous and distinctive spatio-temporal fluctuations, which give rise to a "mosaic structure", with patches of correlated molecules relaxing in a cooperative way [1]. To

develop a complete theory of the glass-transition a detailed picture of the involved microscopic processes is critically required, but yet it is difficult to achieve given the large span of the involved spatial and temporal scales [1,2].

In a deeply supercooled liquid, on decreasing the temperature, the structural (α) relaxation becomes progressively slower until, at T_g, its timescale is of the order of 100 s. [1] At the same time a faster, Arrhenius process, known as Johari-Goldstein (β_{JG}) relaxation, decouples from it at a temperature of $\simeq 1.2\ T_g$, and provides molecular mobility even in the glassy state [2,3]. The β_{JG}-relaxation (not to be con-

fused with the fast β-relaxation envisaged in the mode-coupling theory [4]) is believed to be a fundamental ingredient of the glassy-dynamics, and is strongly connected to the α-relaxation [2,5–7]. "Genuine" β_{JG}-relaxations (as opposed to secondary relaxations arising from intramolecular degrees of freedom [2,7]) are sensitive to the thermodynamic state of the glass [8]. There are also indications of a signature of the β_{JG}-relaxation in the specific heat well below T_g [2,9–14], where the associated degrees of freedom "freeze" [9,15], though different enthalpy-recovery mechanisms could also be involved [16,17]. Concerning the microscopic mechanisms responsible for the β_{JG}-relaxation, recent X-ray scattering experiments and simulations are starting to provide an increasing number of insights. For instance, atomistic simulations of metallic glasses [18,19] have recently connected the β_{JG}-relaxation with string-like motions, while swap Monte Carlo algorithms have paved the way to the equilibration of simulated systems at the relevant timescales for secondary relaxation processes [20].

X-ray [21–25] and neutron scattering experiments [26–28], able to provide length-scale resolved information on the microscopic dynamics, can clearly contribute to the investigation of relaxation processes on approaching T_g. In particular, nuclear γ-resonance time-domain interferometry (TDI) probes microscopic density fluctuations occurring at the timescale where the β_{JG}-process dominates the dynamics [21–25,29,30]. TDI has indeed highlighted the restricted character and anomalous diffusion associated to the β_{JG}-relaxation on approaching T_g [21–24] and allowed to estimate both the average fraction of molecules participating to the process (i.e. the relaxation strength) and their characteristic center-of-mass excursions [23,24]. In fact, evidence was provided that, at the most probable timescale for the β_{JG}-relaxation, the molecules participating to it perform spatial excursions compatible with the Lindemann criterion for structural instability and are therefore able to break the cage formed by their nearest neighbors [24]. Moreover, they form a percolating cluster as their fraction (i.e. the relaxation strength) matches the threshold for site-percolation (which in amorphous liquids can be expected to be around 0.25) [24]. The presence of such a mosaic structure, associated with the β_{JG}-relaxation, is in line with the basic idea of the Random-First Order Transition (RFOT) theory, which also envisages a string-like/percolating topology for the region of the "mosaic" relaxing via the β_{JG}-relaxation [31]. For all these reasons it is intriguing the idea to use the β_{JG}-relaxation as an effective probe of the mosaic structure emerging in the supercooled state aiming at its detailed characterization. In particular, the temperature and inter-molecular potential dependence of the number of molecules participating to the β_{JG}-relaxation (and, thus, of the associated percolating cluster) and their spatial excursions should be investigated in some detail. In fact, we have little information on the relaxation strength of the β_{JG}-relaxation process as it was possible to estimate it so far only for a hydrogen-bonded liquid (5-methyl-2-hexanol [23]).

Motivated by these possibilities, we here report a study of the microscopic properties of the β_{JG}-relaxation for the model van der Waals glass-former cumene using a new TDI scheme with increased efficiency [32]. We find that in cumene roughly 25% of the molecules participates to the cage-breaking events during the β_{JG}-relaxation, thus matching the site percolation threshold. Our results confirm those obtained for the H-bonded liquid 5-methyl-2-hexanol [23] and suggest that the properties of the mosaic structure do not depend on the interaction potential, which is highly directional in the case of H-bonding and more isotropic in the simpler case of van der Waals liquids. Further, we find that the fraction of molecules participating in cage-breaking events during the β_{JG}-relaxation, encoded in the relaxation strength provided by TDI, shows a negligible temperature dependence above T_g.

Our results thus highlight the microscopic properties of the β_{JG}-relaxation that appear more and more universal.

2. Experimental details

Sample Cumene (isopropyl benzene), a model glass-former [33] ($T_g = 127\ K$ [10]) with a genuine β_{JG} relaxation [2,3,10,34], was purchased from Sigma Aldrich and used as received (purity > 99.5%).

Dielectric spectroscopy The re-orientational dynamics of the sample has been characterized using dielectric spectroscopy. In detail the complex permittivity of the sample was measured in the range 10 mHz-10 MHz range using a lumped impedance technique and the Novocontrol Alpha-Analyzer. The sample environment consisted of a dry nitrogen-flow Quatro cryostat with a temperature accuracy better than 0.1 K. The sample cell (in sealed configuration) consisted in a capacitor with parallel plates separated by a sapphire spacer (effective electrode diameter 30 mm, thickness 70-140 μm, empty capacitance 45-90 pF). The cell was filled by the sample in the liquid state.

Time-domain interferometry The microscopic density fluctuations of the sample have been probed by nuclear γ-resonance time-domain interferometry. In a typical TDI experiment two nuclear absorbers, containing the Mössbauer isotope ^{57}Fe, are placed upstream and downstream of the sample [29,35,36]. The nuclear resonance of ^{57}Fe lies at an energy of $\simeq 14.4$ keV, which can be easily excited with synchrotron radiation, and has a lifetime τ_0 (natural linewidth Γ_0) of $\simeq 141$ ns ($\simeq 4.66$ neV), which matches the typical timescales for the β_{JG}-relaxation around T_g. The nuclear absorbers used in TDI usually have different energy spectra. Several approaches can be used to this aim, such as Doppler shifting one absorber with respect to the other [29] or exploiting hyperfine interactions [32,35]. The present experiment was performed at the nuclear resonance beamline ID18 of the European Synchrotron Radiation Facility (ESRF) [37] with the storage ring operating in 4-bunch filling-mode (storage ring current $I = 20\,m$A). In such operation mode the time interval between two synchrotron radiation pulses is 648 ns. A 3-lines setup was used consisting of an α-^{57}Fe foil (thickness 10 μm) to generate the 2-lines probe beam while the reference single-line absorber consisted of a pellet containing K_2Mg^{57}Fe[CN]$_6$ (^{57}Fe surface density: 1 mg/cm^2). To reduce the number of nuclear resonances of α-^{57}Fe to two, we applied a magnetic field of 0.5 T perpendicularly to the horizontal scattering plane, see Refs. [32,36] fore more details. This scheme was chosen because multi-line TDI experiments are indeed more efficient compared to standard 2-lines schemes and allow us to directly extract the relaxation strength of the probed process [35,36].

The TDI signal was simultaneously collected at three different scattering vectors (q) to reduce the total experiment time. In detail, we employed three different groups of APD detectors (time resolution $\simeq 1$ ns), each of them probing a distinct scattering angle. By changing the position of the detectors with respect to the sample we could select the q-values of interest. The temperature of the sample was controlled in a He-flow cryostat with a temperature stability of ± 0.05 K, and all the measurements were performed by directly quenching the sample from above its melting temperature ($T_m = 176\ K$) to the measurement temperature to reduce the probability of crystal nucleation. The absence of crystallization during the data acquisition was monitored by measuring the static structure factor of cumene every 60 minutes.

3. Dielectric spectroscopy measurements

The permittivity function $\epsilon(\nu)$ measured in dielectric spectroscopy (DS) measurements is usually analyzed by jointly fitting its real and imaginary part [38]. The α-relaxation was modeled by a Kohlrausch-Williams-Watts (KWW) function, while we used the Cole-Cole function to describe the β_{JG}-relaxation [38]. More precisely, the α-relaxation was directly fitted with the numerically calculated Laplace transform of the KWW function using the algorithm described in [39]. Fig. 1 shows the dielectric loss (i.e., the imaginary part of $\epsilon(\nu)$) measured at temperatures both above (141 (a) and 136 K (b)) and below (103 K (c)) T_g,
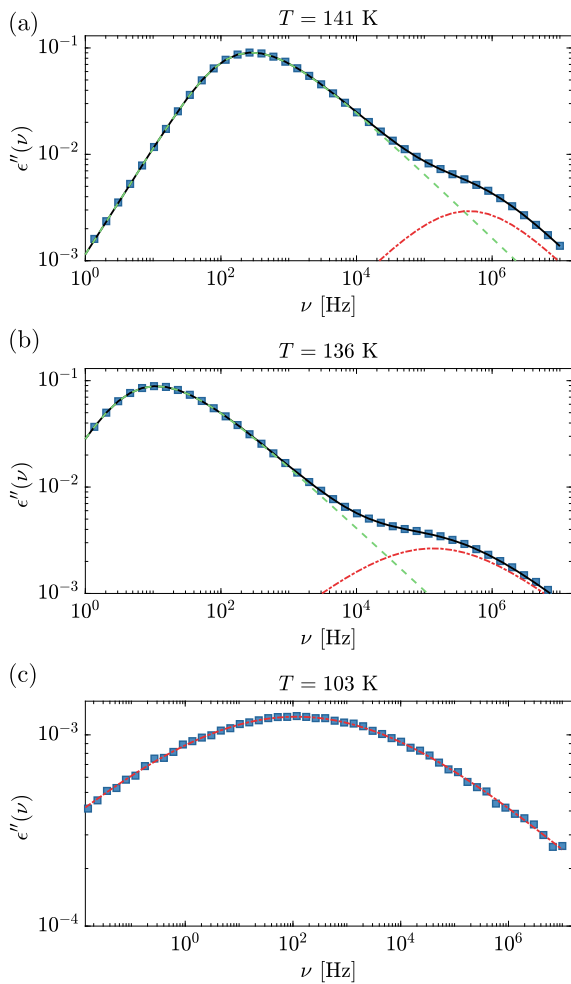
Fig. 1. Dielectric loss spectrum of cumene measured at $T = 141$ K (a), 136 K (b) and 103 K (c). Black solid line: global fit. Green dashed line: contribution of the α-relaxation. Red dash-dotted line: contribution of the β_{JG}-relaxation. At 103 K the β_{JG}-relaxation is the only process present in the experimental frequency window.

along with the global fitting curve (black solid line) and the individual contributions of the α- (green dashed line) and β_{JG}-relaxation (red dash-dotted line) to the spectrum. The β_{JG}-relaxation appears in the dielectric spectra as a high frequency symmetric peak with a dielectric strength usually smaller than the α-relaxation [2] (Fig. 1-(a,b)). Deep in the glassy state the Johari-Goldstein is the only relaxation process still active (see Fig. 1-(c)) and has a larger dispersion compared to the spectra at higher temperatures, as observed in many glass-formers [2].

4. Time-domain interferometry measurements

In a TDI experiment, the first nuclear absorber can be regarded as a split and delay line: a γ-photon impinging onto it can be either transmitted or resonantly absorbed by the long-living nuclear resonance of ^{57}Fe. These two scattering paths are coherently coupled. The second absorber, given its different excitation spectrum, acts as reference or phase-sensitive analyzer: when the scattering paths recombine at the downstream absorber, a time-domain pattern of quantum beats arises, with a period and structure depending on the energy spectra of the two absorbers. For example, in the current experiment the interferogram consists of two groups of quantum beats with frequency $\Omega \simeq 60\Gamma_0$ and $\Omega/2 \simeq 30\Gamma_0$, respectively [32]. Since the coherent superposition of the paths is mediated by the scattering from the sample placed in between the two absorbers, quasi-elastic scattering events in the sample
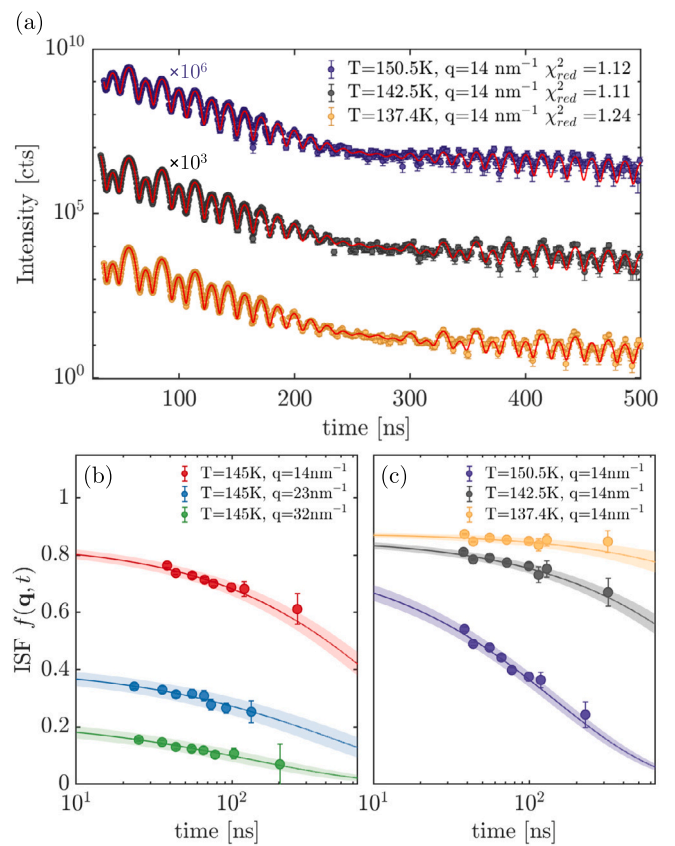

Fig. 2. (a): time-domain interferometry beating patterns of cumene at $q = 14$ nm^{-1} (corresponding roughly to the intermolecular distance) at different temperatures. The symbols with errorbars are the experimental data, while the red-solid lines are the model curves obtained from the fitting procedure. To increase the visibility, the beating patterns at $T = 137.4$ K and 150.5 K have been scaled by a factor 10^3 and 10^6, respectively. (b): Intermediate scattering functions (ISFs or $f(\mathbf{q},t)$) obtained from the time-domain interferograms at different scattering-vectors (q) at a fixed temperature. (c): ISFs extracted from the time-domain interferograms measured at fixed (q) and different temperatures. The solid curves in (b) and (c) are the ISF obtained by fitting the interferograms, while the symbols with errorbars show the ISF directly extracted from the experimental data. The shaded areas show the 68% confidence intervals.

lead to a loss of phasing and a consequent damping of the beating pattern [29,35,36]. In the specific case of the 3-line scheme used here, quasi-elastic scattering in the sample reduces the contrast between the beatings with frequencies Ω and $\Omega/2$ (see for example Fig. 2-(a)).

The time evolution of the beating pattern can be quantitatively described using for the intensity measured for a scattering vector q and at time t the model introduced in Refs. [32,36]:

$$\bar{I}(\mathbf{q},t) = |R_A(t)|^2 + |R_B(t)|^2 \cdot f_{\Delta E}(\mathbf{q}) + 2Re\{R_A(t,T) \cdot R_B(t,T)\} f(\mathbf{q},t). \quad (1)$$

In Eq. (1) $R_{A,B}(t)$ are the responses of the probe (two-line, A) and reference (single-line, B) absorber, respectively; $f(\mathbf{q},t)$ is the normalized density, $\rho(\mathbf{q},t)$, correlation function or intermediate scattering function:

$$f(\mathbf{q},t) = \frac{\langle \rho(\mathbf{q},0)\rho(\mathbf{q},t)\rangle}{\langle |\rho(\mathbf{q},0)|^2 \rangle} \quad (2)$$

and $f_{\Delta E}$ a parameter depending both on sample properties and on the bandwidth of the incident radiation [35]. More details on the models used to describe $R_{A,B}(t)$ can be found in [32,36]. $R_{A,B}(t)$ are usually calibrated in absence of the sample or, as in the present case, from interferograms measured at a temperature (25 K) well below T_g where the sample shows no dynamics. This approach allows us also to estimate possible losses of coherence of instrumental origin. $f_{\Delta E}$ and $f(\mathbf{q},t)$ are

instead extracted via a fitting procedure to the beating patterns. It is important to point out that $f_{\Delta E}$ and $f(\mathbf{q},t)$ can be separated in the fitting procedure only when $|R_A(t)|$ and $|R_B(t)|$ are different [35], a condition that is naturally achieved in a 3-line TDI scheme [36].

The intermediate scattering function is usually described by the KWW function [2] as it provides a good account of the experimental data [21,24]:

$$f(\mathbf{q},t) = f_q \exp\left[-\left(\frac{t}{\tau(\mathbf{q},t)}\right)^{\beta_{KWW}}\right]. \tag{3}$$

In Eq. (3), f_q is the relaxation strength (i.e. the fraction of molecules participating to the relaxation process), $\tau(\mathbf{q})$ the relaxation time of the density fluctuations and β_{KWW} is the stretching parameter. While the α- and the β_{JG}-relaxations show different spectral shapes in dielectric spectra [2], using the single shape of Eq. (3) independently of the details of the underlying dynamical process is here preferred as it introduces a minimal bias in the fitting procedure. Furthermore, as also discussed in the methods section of Ref. [24], TDI beating patterns span less than two decades in time and are not much sensitive to the stretched tails characteristic of the Cole-Cole susceptibility in the time-domain. For the same reason, the relaxation parameters are rather insensitive to the exact shape of the model selected for describing the intermediate scattering function.

The relatively small time-window of TDI does not allow leaving free all three parameters entering Eq. (3). Therefore, in the fitting procedure for all beating patterns measured at $q \neq q_{max}$ =14 nm^{-1}, the coefficient β_{KWW} was fixed to the average value (β_{KWW} = 0.56) obtained from our dielectric spectroscopy measurements of the structural relaxation, similarly to what reported in Refs. [21,23,24]. Here, q_{max} is the q-value corresponding to the strongest peak of the scattered intensity, $I(q)$. For what concerns the data collected at q_{max}, the parameter β_{KWW} was increased by 20% ($\beta_{KWW}(q_{max})$ = 0.67) in order to account for the q-dependence expected in the case of the α-relaxation [23,24]. It is indeed well-known, thanks to numerical simulations [40,41] and experiments [42,43], that the α-relaxation shape parameter β_{KWW} becomes larger on approaching the peak of the static structure factor (meaning that the associated distribution of relaxation times is narrower). The same trend is here assumed to hold independently of the dynamical process caught by the model of Eq. (3), i.e. independently of whether the process probed by TDI is the $\alpha-$ or the β_{JG}-relaxation. This approach clearly introduces the minimum bias in the fitting analysis when it is of interest to understand which relaxation process is being probed. Further, while the q-dependence of the stretching parameter for the β_{JG}-relaxation is not known, it is not unreasonable to expect a somewhat narrower distribution of relaxation times at the inter-molecular length-scale also for the β_{JG}-relaxation, due to the fact that inter-molecular correlations are the strongest at that point.

The tenability of this assumption was checked by jointly fitting in a preliminary analysis the model of Eq. (1) to the experimental data for each q-value and at all temperatures, leaving the β_{KWW} as a global free parameter. This analysis provides the following estimates for β_{KWW}: 0.5(2) at q = 14 nm^{-1} and 0.5(2) at q = 23 and 32 nm^{-1}, compatibly with our assumptions. Clearly, this fitting procedure leads to larger uncertainties in the fitting parameters than fixing the shape of the intermediate scattering function. In what follows we will describe the results obtained fitting Eq. (3) to each measured interferogram separately with the $\beta_{KWW}(q_{max})$ parameter fixed as explained above.

Fig. 2-(a) shows, as an example, a few TDI beating patterns measured on cumene along with the fitting curves (red solid lines). Fig. 2-(b) (c) reports the $T(q)$ dependence of $f(\mathbf{q},t)$ while keeping $q(T)$ fixed. The solid lines are the KWW functions best fitting the interferograms while the circles with errorbars show the $f(\mathbf{q},t)$ values resulting from the procedure reported in Ref. [35]. Briefly, $f(\mathbf{q},t)$ is obtained using Eq. (1), by subtracting the experimental responses of the probe and reference absorbers, and after fixing $f_{\Delta E}$ to the value extracted from the fitting
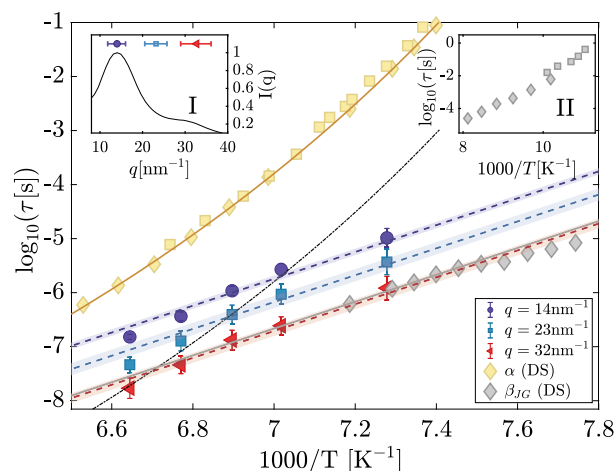

Fig. 3. Relaxation map obtained from time-domain interferometry and dielectric spectroscopy measurements. Inverse temperature dependence of the relaxation time (τ) measured by dielectric spectroscopy (yellow and grey diamonds) and time-domain interferometry at three different q-values: 14 (violet circles), 23 (cyan squares) and 33 (red left-pointing triangles) nm^{-1}. The structural relaxation time from Ref. [44] is also reported for comparison (yellow squares). The solid lines are fits to the dielectric spectroscopy data. The α-relaxation is fitted using the Vogel-Fulcher-Tammann equation while the β_{JG}-relaxation using the Arrhenius one. The time-domain interferometry (TDI) relaxation-times are fitted by scaling the Arrhenius T-dependence obtained from the dielectric spectroscopy data (dashed lines through the data, with the shaded areas corresponding to the 68% confidence interval). The black dashed-dotted line is the T-dependence obtained from the dielectric spectroscopy data for the α-relaxation and rescaled to match the TDI value at 32 nm^{-1} and at the highest probed temperature. Inset (I): Total scattering intensity as a function of the exchanged wave-vector q. The markers with horizontal errorbars show the q-points investigated and the corresponding q-range. Inset (II): T-dependence the β_{JG} relaxation time as measured by dielectric spectroscopy below T_g. Gray diamonds: present work; gray squares: data from Ref. [44].

procedure. The resulting data points are then binned with a logarithmic spacing and the uncertainty is calculated by performing a weighted average within each bin. This method allows us to directly extract the intermediate scattering function from the data: a good agreement between the data and the fitted KWW functions can be observed, further validating our analysis.

5. Relaxation map and temperature dependence of the relaxation strength

The temperature dependence of τ was investigated for three different q-values (see inset (I) of Fig. 3): 14 nm^{-1} (violet circles), corresponding to the average intermolecular distance, 23 nm^{-1} (cyan squares) and 32 nm^{-1} (red triangles). The measured τ values are plotted in Fig. 3 along with the ones obtained by dielectric spectroscopy (DS, yellow and gray diamonds), which probes the molecular re-orientational dynamics. The DS spectroscopy data provide a precise estimation of the T-dependence of the relaxation time of both the α and β_{JG}-process that can hence be used as a fingerprint to search for these processes in the TDI data. In Fig. 2 we also report the DS relaxation times from Ref. [44]: the yellow squares in the main plot are the relaxation times of the α-process while the τ-values corresponding to the β_{JG}-relaxation are compared with ours, below T_g, in the inset II. In both cases a nice agreement can be observed.

Concerning the TDI data, τ shows a simple Arrhenius temperature dependence at all q-values, consistent with the one of the β_{JG}-process from the DS data (especially at $T < 147$ K). This is shown by the dashed lines in Fig. 3, obtained by re-scaling the temperature dependence obtained from the DS data onto the TDI data. This means that in the probed q- and T-range we are mostly sensitive to the β_{JG}-relaxation.
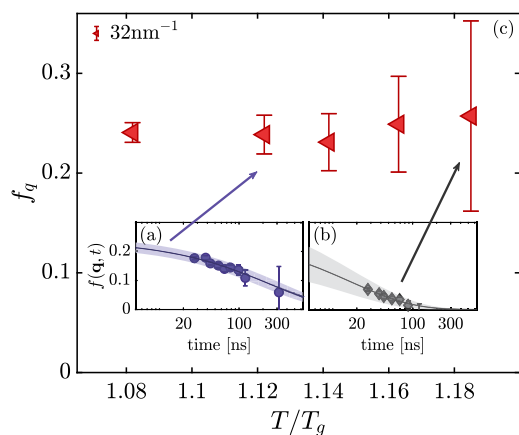
Fig. 4. (a,b): intermediate scattering functions extracted at q =32 nm^{-1} and T =142.5 K and 150.5 K, respectively. (c): temperature dependence of the relaxation strength of the Johari-Goldstein relaxation at q =32 nm^{-1}.

In fact, if we re-scale the temperature dependence of the α-relaxation obtained from DS onto the TDI data (see, for example, the black dashed-dotted line in Fig. 3) we cannot satisfactorily describe the TDI data. We underline that our measurements were performed at temperatures between 1.17 and 1.09 T_g and usually the α and β_{JG}-relaxation decouple around $1.2T_g$. We could not explore higher temperatures than those reported in Fig. 3 due to sample crystallization.

It is important to stress that cumene, despite being a small molecule, possesses internal degrees of freedom (related to the isopropyl chain) which could in principle couple to density fluctuations at a local scale. However, this possible coupling that can be neglected here by considering that: i) the timescale found at the intra-molecular length-scale is in close agreement with the one provided by DS for the β_{JG}-relaxation, ii) the same activation energy is found at both the inter and intra-molecular scale, and iii) a strong scattering vector (length-scale) dependence of the characteristic relaxation time is found (see discussion in Sec. 6). In fact, density fluctuations associated to an internal degree of freedom should give rise to a q-independent relaxation time. Furthermore, nuclear magnetic resonance (NMR) studies show that iv) the dynamics of the benzene ring and of the iso-propyl group of cumene are strongly coupled down to T_g [45], and the activation energy for methyl-group rotations is around $\simeq 0.14$ eV ($\simeq 14$ kJ/mol) [46]. This value is sensibly different from the one of $\simeq 0.4$ eV here found for the density fluctuations. Therefore, we can safely conclude that we are sensitive to the center-of-mass dynamics of the system within the β_{JG}-relaxation, rather than to an intra-molecular motion.

As already observed in other glass-formers [23,24], the timescale of molecular re-orientations within the β_{JG}-relaxation (as probed by DS) matches that for microscopic density fluctuations at a q-value $q_{DS} \simeq 32$ nm^{-1}, above the peak of the static structure factor $q_{max} = 14$ nm^{-1}. This q_{DS} value identifies the most-probable mean-squared displacement at the timescale of molecular re-orientations [23,24], and corresponds to a well defined fraction of the inter-molecular distance (more details in Sec. 6). We also notice that the intermediate scattering function decorrelates completely via the β_{JG} process at $q_{DS} = 32$ nm^{-1} (see for example Fig. 4-(a,b)): this means that at such q-value the β_{JG}-relaxation dominates slow density fluctuations, while the α process is either not present or has a negligible strength. Concerning $q = 14$ nm^{-1} and 23 nm^{-1}, we don't directly observe the full de-correlation of the intermediate scattering function, and the structural relaxation might still relax the density fluctuations at times longer than those where we have access, and this especially at the inter-molecular scale. For instance, even at the highest accessible temperature ($T = 150.5$ K) we could observe density fluctuations de-correlating only by 50% at $q = 14$ nm^{-1} (see Fig. 1-(c)).
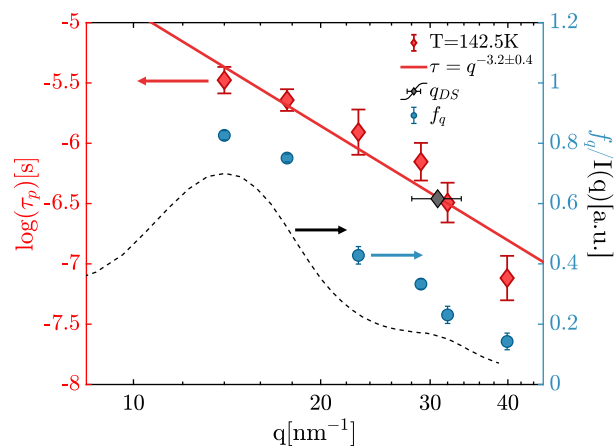

Fig. 5. Left y-axis: scattering vector (q) dependence of the characteristic relaxation time τ_q (red diamonds with errorbars) measured at T =142.5 K. τ_q is extracted from the peak position of the susceptibility function of density fluctuations. The red solid line is obtained fitting a power-law $\tau \propto q^{-n}$ to the experimental data. The black diamond with errorbar marks the q-value, q_{DS}, at which the TDI and DS relaxation times match at T =142.5 K. Right y-axis: q-dependence of the relaxation strength (f_q) (blue circles with errorbars) and of the total scattering intensity (black dashed line).

At $q = 32$ nm^{-1}, where it is safe to assume that only the β_{JG}-relaxation is active, we can extract its relaxation strength $f_{JG}(q_{DS})$. As it is possible to observe in Fig. 4-(c), $f_{JG}(q_{DS})$ does not show a pronounced temperature dependence, remaining $\simeq 0.25$ in the whole explored temperature range. This value is in agreement with our previous estimate for 5M2H [23]. We underline, however, that in the present case we can directly extract f_q and probe its temperature dependence thanks to the multi-line TDI setup which allows us to separately extract $f(\mathbf{q},t)$ (and thus f_q), and $f_{\Delta E}$ (see also discussions in Refs. [35,36]).

6. q-dependence

The scattering vector (q) dependence of the relaxation parameters provides detailed information on the microscopic motions involved in the β_{JG}-relaxation. The q-dependence of the relaxation time and strength, f_q, are plotted in Fig. 5. In order to facilitate the comparison to the DS results, the relaxation times reported here and extracted from the TDI interferograms have been converted to those, τ_p, corresponding to the peak of the susceptibility function, following the procedure in Ref. [24]. In fact, the TDI and the DS data were fitted with different models, namely the KWW function (Eq. (3)) and the Cole-Cole function, respectively, as discussed in Sec. 2 and 3. In the case of the Cole-Cole function, used for the DS data, the relaxation time of the β_{JG} process ($\tau_{\beta_{JG}}^{DS}$) is identified by the angular frequency position of the susceptibility peak (ω_p):

$$\tau_{\beta_{JG}}^{DS} = \frac{1}{\omega_p}. \tag{4}$$

In the case of TDI, which is fitted in the time-domain using the KWW model, τ is not directly related to the peak of the corresponding susceptibility (ω_p^{KWW}): ω_p^{KWW} is indeed located at slightly lower frequencies than $1/\tau(q)$. To facilitate the comparison between the results of the two techniques we therefore transformed τ into τ_p:

$$\tau_p = \frac{1}{\omega_p^{KWW}}. \tag{5}$$

In detail, we computed the susceptibility corresponding to Eq. (3) using the algorithm described in Ref. [39] (the KWW equation has no analytical Fourier/Laplace transform) and then we numerically found τ_p.

The results for τ_p and f_q reported in Fig. 5 show that both parameters change significantly with q, and both show a modulation with

q similar to the total scattering intensity, $I(q)$. More in detail, the q-dependence of τ_q can be fitted using a power law $\tau_p \propto q^{-n}$, which results in $n = 3.2(4)$. Such super-quadratic q-dependence, which seems characteristic of the β_{JG}-relaxation [21,23,24], indicates sub-diffusive dynamics: this means that motions within the β_{JG}-relaxation are highly restricted, with the associated mean-squared displacement increasing sub-linearly with time.

We also observe that n is slightly smaller than in the case of mono-hydroxyl alcohols [23,24] ($n_{alc} \approx 4$) and similar to what observed for o-terphenyl [21] above T_g ($n_{OTP} = 2.9(5)$). This might suggest that the sub-diffusive character of the β_{JG}-relaxation depends on the interaction potential and it is more pronounced (larger n) in systems with directional bonds.

The q-dependence of τ_p can also be used to identify the scattering vector, q_{DS}, at which the timescale for density fluctuations, probed by TDI, and molecular re-orientations ($\tau^{DS}_{\beta_{JG}}$), probed by DS, match [24]. q_{DS} identifies then the most-probable length-scale for molecular center-of-mass displacements at $\tau^{DS}_{\beta_{JG}}$. In fact, TDI can be used to spatially resolve the distribution of relaxation times of the β_{JG}-relaxation probed by techniques sensitive to the re-orientational dynamics, such as DS and photon correlation spectroscopy, as discussed in Ref. [47].

The obtained value of q_{DS} allows us to calculate the most-probable root-mean-squared displacement Δr_{JG} occurring at $\tau^{DS}_{\beta_{JG}}$ using an anomalous diffusion model within the Gaussian approximation [24]. Briefly, our measurements show that the intermediate scattering function at q_{DS} is well described by a KWW function. Therefore, if we i) account for the super-quadratic q-dependence of τ:

$$\tau(q) = \tilde{D}^{-\frac{n}{2}} q^{-n}, \tag{6}$$

where $\tilde{D}$ is a generalized diffusion coefficient [24], and ii) neglect the q-dependence of f_q around q_{DS}, we can write:

$$f(q_{DS}, t) \approx \exp\left[-\left(\tilde{D}^{\frac{n}{2}} q^n t\right)^{\beta_{KWW}}\right]. \tag{7}$$

Since $n \cdot \beta_{KWW} = 1.8(2) \approx 2$, it is clear that $f(q_{DS}, t)$ results to be approximately Gaussian in q, at least at $\tau^{DS}_{\beta_{JG}}$ and around q_{DS}:

$$f(q_{DS}, t) \approx \exp\left[-\tilde{D} t^{\beta_{KWW}} q^2\right]. \tag{8}$$

Within this approximation, the mean-squared displacement can be written as:

$$\langle r^2(t) \rangle = 6\tilde{D} t^{\beta_{KWW}}, \tag{9}$$

making it possible to relate q_{DS} to the mean-squared displacement at $\tau_{\beta_{JG}}$ [24]:

$$\Delta r_{JG} = \sqrt{\langle r^2(\tau^{DS}_{\beta_{JG}}) \rangle} = \frac{\sqrt{6}}{q_{DS}} = 0.80(7) \text{ Å}, \tag{10}$$

where the factor 6 accounts for the fact that we are modelling the process in three dimensions.

Δr_{JG} results to be roughly 13% of the average inter-molecular distance as estimated from the molecular volume. This result is similar to what previously reported for 5-methyl-2-hexanol, 1-propanol and o-terphenyl [24].

7. Discussion

The β_{JG}-relaxation of cumene displays, analogously to other previously investigated glass-formers [23,24] a strong super-quadratic q-dependence and dominates the microscopic dynamics at large scattering vectors, where density fluctuations relax via a sub-diffusive motion. Moreover, the characteristic MSD, Δr_{JG}, evaluated at the most-probable timescale for re-orientations, satisfies the Lindemann criterion for structural instability. According to the Lindemann criterion, molecular displacements of around 10% of the inter-particle distance from
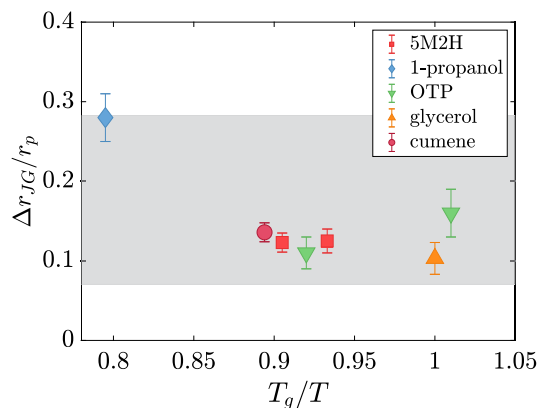

Fig. 6. Inverse temperature dependence of the characteristic center-of-mass displacement Δr_{JG} at the β_{JG}-relaxation characteristic time of the molecules participating to the β_{JG}-relaxation, rescaled to the average intermolecular distance, r_p. The gray area shows the range of typical values for the Lindemann criterion in crystals (see ref. [49] and references therein) expressed in terms of root-mean-squared displacement, as also discussed in Ref. [24].

equilibrium positions, lead to structural instability/melting, a condition, as discussed also in [24], which is met by the molecules taking part to the β_{JG}-relaxation at $\tau^{DS}_{\beta_{JG}}$. This then implies that also in cumene the molecules involved in the β_{JG}-relaxation perform, at $\tau^{DS}_{\beta_{JG}}$, critical-amplitude displacements in the cage formed by their nearest neighbors, leading therefore to cage breaking events. It is interesting to notice that the quasi-local character of the β_{JG}-relaxation has also been suggested by recent experiments on polyamorphic metallic glasses showing the β_{JG}-relaxation to be mainly sensitive to short-range order [48].

Fig. 6 shows Δr_{JG}, normalized to the center-of-mass to center-of-mass distance (r_p) and as a function of the inverse temperature, for cumene and all other glass-formers for which this information is available and that belong to the H-bonded [23–25] and van der Waals classes of liquids [21]. With the exception of propanol, which was probed at a temperature sensibly higher than T_g, the molecular excursions at $\tau^{DS}_{\beta_{JG}}$ of the molecules participating in the β_{JG}-relaxation and at temperatures close to T_g are all of the order of 12%-13% of the nearest neighbors distance. This result suggests the universal character of the β_{JG} relaxation as a cage-breaking process. In fact, the amplitude of these motions satisfies the Lindemann criterion for structural instability and they are therefore expected to break the cages formed be the nearest neighbors [24,49].

It is in particular intriguing that also the recent TDI results for glycerol [25], though of more difficult interpretation [50] as the contribution of the β_{JG} relaxation to the dielectric spectra (if present at all) is still debated [51–53], also agree with this scenario when analyzed within our scheme.

The present measurements on cumene provide also a detailed characterization of the temperature dependence of the strength of the β_{JG}-relaxation, extending previous results on 5-methyl-2-hexanol [23] and thanks to an improved experimental scheme [32]. In particular, we find here that $f_{JG}(q_{DS}) \simeq 0.25$ in the whole probed temperature range, see Fig. 4. This suggests that the fraction of molecules undergoing cage-breaking events is not strongly affected by temperature (at least above T_g) and by the molecular interaction potential as the same fraction of molecules ($\simeq 25\%$) contribute to the β_{JG}-relaxation at $\tau^{DS}_{\beta_{JG}}$ both in H-bonding and van der Waals liquids.

At timescales longer than $\tau^{DS}_{\beta_{JG}}$ and before the onset of the structural relaxation a fraction of these more mobile molecules, escaping from the cage formed by the nearest neighbors, are eventually able to (sub) diffuse to longer distances [24,23]. It is reasonable to expect that these larger spatial excursions are associated to the string-like reconfiguring regions observed in metallic glasses [18,19]).

The weak dependence of $f_{JG}(q_{DS})$ on T, at a first glance, seems to be at odds with what usually observed by dielectric spectroscopy: as often reported in the literature, the dielectric strength of the β_{JG}-process decreases on approaching T_g [2,54]. This apparent discrepancy is easily justified by the fact that TDI provides a different perspective compared to dielectric spectroscopy. The dielectric strength depends on both the number of relaxing dipoles and on the amplitude of the angular excursions which is temperature dependent as well. [2,55,56]. On the contrary, f_{JG} corresponds to the fraction of molecules that at τ have moved over a distance fixed by the scattering vector q (i.e. $\simeq 1/q$). So f_{JG} directly reflects the molecular participation to a relaxation process at a given q. Further, while dielectric spectroscopy provides a spatially averaged information, TDI allows to selectively probe different microscopic length-scales (identified by q). For these reasons our results present a complementary and more direct picture of the microscopic motions taking place during the β_{JG}-relaxation.

We also stress that the temperature independence of f_{JG} has been observed only in a specific q-region around 32 nm^{-1} which corresponds to the characteristic scale for cage-breaking events. So, our results show that the fraction of molecules able to locally change the amorphous structure is independent of the temperature. We cannot conclude the same for larger spatial excursions (i.e., density fluctuations at smaller q-values), which are likely to be accompanied by larger angular reorientations in view of the roto-translation coupling discussed in [23]). In fact, at $q < 32$ nm^{-1} the molecular dynamics is too slow for the time-window directly accessed by TDI: at these q-values we cannot rule out the presence of the structural relaxation and thus we cannot investigate the temperature dependence of f_{JG} alone. We can however expect these longer-range excursions to be more sensitive to temperature and to be strongly reduced on approaching T_g, and the more so in the glassy state. For the same reason it is also reasonable to anticipate a reduction of these longer-ranged molecular rearrangements during isobaric and isothermal aging or when an ultra-stable glass is produced, in line with the sensitivity of the β_{JG}-relaxation to the thermodynamic state of the glass [2,3,8].

It is interesting to notice that our results are compatible with the picture proposed in Ref. [57] where, based on thermodynamic considerations, it is argued that regions with a higher-than-average mobility are at the origin of the β_{JG}-relaxation in the glassy state. In fact, our microscopic description of the β_{JG}-relaxation shares several similarities with models that suggest the β_{JG}-relaxation to be associated with liquid-like regions and that are based on investigations of sub-T_g crystallization [58,59] or stress/surface defects relaxation in metallic glasses. [60–62]. Moreover, in Ref. [59] the fraction of molecules in such liquid-like regions has been derived from the crystallized fraction of the metallic glass after ultrasound annealing and results to be roughly 20%, in agreement with our results. However, a direct comparison of this estimation with our microscopic results requires caution since it relies on the delicate assumption that the crystallized domains observed in Ref. [59] are entirely due to molecules participating only in the β_{JG}-relaxation. We also notice that in Ref. [60], it is reported that the onset of macroscopic flow in the glassy-state, which is there associated with the activation of the β_{JG}-relaxation, occurs only when the fraction of liquid-like zones reaches 0.25 (i.e. the percolation threshold for the system). Even though a direct connection with our microscopic results is, again, not straightforward, it is nonetheless interesting to notice that also macroscopic flow measurements suggest that the occurrence of the β_{JG}-relaxation is associated with a percolating structure.

8. Conclusions

In conclusion, we studied the microscopic properties of the β_{JG}-relaxation in the van der Waals liquid cumene using nuclear γ-resonance time-domain interferometry. Our investigation, covering a wide range of scattering vectors (13–40 nm^{-1}) and timescales (10^{-9}–10^{-5} s), shows that in cumene the β_{JG}-relaxation dominates the den-

sity fluctuations at intra-molecular distances and that its characteristic mean-squared displacement is $\simeq 13\%$ of the average intermolecular distance, in line with previous observations. This confirms that the molecules participating in the β_{JG}-relaxation are able to break the cages formed by the nearest neighbors before the structural relaxation occurs. Moreover, thanks to the extended dynamic range of our detection scheme we could directly measure the relaxation strength of the β_{JG}-relaxation and found that it weakly depends on temperature, being $\simeq 0.25$ in the whole probed temperature range. The fraction of cage-breaking molecules participating to the β_{JG}-relaxation does not decrease on approaching T_g when evaluated at $\tau_{\beta_{JG}}$. In other words, while the time required for cage-breaking events, i.e. $\tau_{\beta_{JG}}^{DS}$, increases while approaching T_g, the topology of the percolating cluster (identified by the fraction of involved molecules) is weakly dependent on temperature. Moreover, the value obtained for the relaxation strength confirms previous estimates for H-bond liquids, showing that the properties of the percolating cluster do not depend on the molecular interaction potential.

CRediT authorship contribution statement

Federico Caporaletti: Conceptualization, Formal analysis, Investigation, Supervision, Visualization, Writing – original draft, Writing – review & editing. **Simone Capaccioli:** Conceptualization, Formal analysis, Visualization, Writing – review & editing. **Dimitrios Bessas:** Investigation, Resources, Writing – review & editing. **Aleksander I. Chumakov:** Investigation, Resources, Writing – review & editing. **Alessandro Martinelli:** Investigation, Writing – review & editing. **Giulio Monaco:** Conceptualization, Formal analysis, Project administration, Supervision, Writing – original draft, Writing – review & editing.

Declaration of competing interest

The authors declare that they have no known competing financial interests or personal relationships that could have appeared to influence the work reported in this paper.

Data availability

Data will be made available on request.

Acknowledgements

References

[1] L. Berthier, G. Biroli, Theoretical perspective on the glass transition and amorphous materials, Rev. Mod. Phys. 83 (2) (2011) 587.

[2] K. Ngai, Relaxation and Diffusion in Complex Systems, Springer Science & Business Media, 2011.

[3] G.P. Johari, M. Goldstein, Viscous liquids and the glass transition. II. Secondary relaxations in glasses of rigid molecules, J. Chem. Phys. 53 (6) (1970) 2372–2388.

[4] W. Götze, Complex Dynamics of Glass-Forming Liquids: A Mode-Coupling Theory, vol. 143, Oxford University Press on Demand, 2009.

[5] K. Ngai, Relation between some secondary relaxations and the α relaxations in glass-forming materials according to the coupling model, J. Chem. Phys. 109 (16) (1998) 6982–6994.

[6] S. Capaccioli, M. Paluch, D. Prevosto, L.-M. Wang, K. Ngai, Many-body nature of relaxation processes in glass-forming systems, J. Phys. Chem. Lett. 3 (6) (2012) 735–743.

[7] K. Ngai, M. Paluch, Classification of secondary relaxation in glass-formers based on dynamic properties, J. Chem. Phys. 120 (2) (2004) 857–873.

[8] H. Yu, M. Tylinski, A. Guiseppi-Elie, M. Ediger, R. Richert, Suppression of β relaxation in vapor-deposited ultrastable glasses, Phys. Rev. Lett. 115 (18) (2015) 185501.

[9] Q. Yang, S.-X. Peng, Z. Wang, H.-B. Yu, Shadow glass transition as a thermodynamic signature of β relaxation in hyper-quenched metallic glasses, Nat. Sci. Rev. 7 (12) (2020) 1896–1905.

[10] K. Kishimoto, H. Suga, S. Seki, Calorimetric study of the glassy state. VIII. Heat capacity and relaxational phenomena of isopropylbenzene, Bull. Chem. Soc. Jpn. 46 (10) (1973) 3020–3031.

[11] J. Fan, E. Cooper, C. Angell, Glasses with strong calorimetric. beta.-glass transitions and the relation to the protein glass transition problem, J. Phys. Chem. 98 (37) (1994) 9345–9349.

[12] N.G. Perez-De Eulate, D. Cangialosi, The very long-term physical aging of glassy polymers, Phys. Chem. Chem. Phys. 20 (18) (2018) 12356–12361.

[13] M. Gao, J. Perepezko, Separating β relaxation from α relaxation in fragile metallic glasses based on ultrafast flash differential scanning calorimetry, Phys. Rev. Mater. 4 (2) (2020) 025602.

[14] R. Androsch, K. Jariyavidyanont, C. Schick, Enthalpy relaxation of polyamide 11 of different morphology far below the glass transition temperature, Entropy 21 (10) (2019) 984.

[15] K. Ngai, S. Capaccioli, D. Prevosto, L.-M. Wang, Coupling of caged molecule dynamics to JG β-relaxation III: van der Waals glasses, J. Phys. Chem. B 119 (38) (2015) 12519–12525.

[16] X. Monnier, J. Colmenero, M. Wolf, D. Cangialosi, Reaching the ideal glass in polymer spheres: thermodynamics and vibrational density of states, Phys. Rev. Lett. 126 (11) (2021) 118004.

[17] Z. Song, C. Rodríguez-Tinoco, A. Mathew, S. Napolitano, Fast equilibration mechanisms in disordered materials mediated by slow liquid dynamics, Sci. Adv. 8 (15) (2022) eabm7154.

[18] H.-B. Yu, R. Richert, K. Samwer, Structural rearrangements governing Johari-Goldstein relaxations in metallic glasses, Sci. Adv. 3 (11) (2017) e1701577.

[19] H.-B. Yu, M.-H. Yang, Y. Sun, F. Zhang, J.-B. Liu, C.-Z. Wang, K.-M. Ho, R. Richert, K. Samwer, Fundamental link between β relaxation, excess wings, and cage-breaking in metallic glasses, J. Phys. Chem. Lett. 9 (19) (2018) 5877–5883.

[20] B. Guiselin, C. Scalliet, L. Berthier, Microscopic origin of excess wings in relaxation spectra of supercooled liquids, Nat. Phys. 18 (4) (2022) 468–472.

[21] M. Saito, S. Kitao, Y. Kobayashi, M. Kurokuzu, Y. Yoda, M. Seto, Slow processes in supercooled o-terphenyl: relaxation and decoupling, Phys. Rev. Lett. 109 (11) (2012) 115705.

[22] T. Kanaya, R. Inoue, M. Saito, M. Seto, Y. Yoda, Relaxation transition in glass-forming polybutadiene as revealed by nuclear resonance x-ray scattering, J. Chem. Phys. 140 (14) (2014) 144906.

[23] F. Caporaletti, S. Capaccioli, S. Valenti, M. Mikolasek, A. Chumakov, G. Monaco, A microscopic look at the Johari-Goldstein relaxation in a hydrogen-bonded glass-former, Sci. Rep. 9 (1) (2019) 1–10.

[24] F. Caporaletti, S. Capaccioli, S. Valenti, M. Mikolasek, A. Chumakov, G. Monaco, Experimental evidence of mosaic structure in strongly supercooled molecular liquids, Nat. Commun. 12 (1) (2021) 1–7.

[25] M. Saito, M. Kurokuzu, Y. Yoda, M. Seto, Microscopic observation of hidden Johari-Goldstein-β process in glycerol, Phys. Rev. E 105 (1) (2022) L012605.

[26] P. Luo, Y. Zhai, P. Falus, V. García Sakai, M. Hartl, M. Kofu, K. Nakajima, A. Faraone, et al., Q-dependent collective relaxation dynamics of glass-forming liquid ca0. 4k0. 6 (no3) 1.4 investigated by wide-angle neutron spin-echo, Nat. Commun. 13 (1) (2022) 1–9.

[27] M.T. Cicerone, Q. Zhong, M. Tyagi, Picosecond dynamic heterogeneity, hopping, and Johari-Goldstein relaxation in glass-forming liquids, Phys. Rev. Lett. 113 (11) (2014) 117801.

[28] M.T. Cicerone, M. Tyagi, Metabasin transitions are Johari-Goldstein relaxation events, J. Chem. Phys. 146 (5) (2017) 054502.

[29] A. Baron, H. Franz, A. Meyer, R. Rüffer, A. Chumakov, E. Burkel, W. Petry, Quasielastic scattering of synchrotron radiation by time domain interferometry, Phys. Rev. Lett. 79 (15) (1997) 2823.

[30] G. Smirnov, U. Van Buerck, H. Franz, T. Asthalter, O. Leupold, E. Schreier, W. Petry, Nuclear γ resonance time-domain interferometry: quantum beat and radiative coupling regimes compared in revealing quasielastic scattering, Phys. Rev. B 73 (18) (2006) 184126.

[31] J.D. Stevenson, P.G. Wolynes, A universal origin for secondary relaxations in supercooled liquids and structural glasses, Nat. Phys. 6 (1) (2010) 62–68.

[32] F. Caporaletti, A. Chumakov, R. Rüffer, G. Monaco, A new experimental scheme for nuclear γ-resonance time-domain interferometry, Rev. Sci. Instrum. 88 (10) (2017) 105114.

[33] H.W. Hansen, B. Frick, S. Capaccioli, A. Sanz, K. Niss, Isochronal superposition and density scaling of the α-relaxation from pico-to millisecond, J. Chem. Phys. 149 (21) (2018) 214503.

[34] K. Ngai, M.S. Thayyil, L.-M. Wang, Quasielastic neutron scattering evidence of coupling of caged molecule dynamics to JG β-relaxation, J. Mol. Liq. 247 (2017) 300–303.

[35] M. Saito, R. Masuda, Y. Yoda, M. Seto, Synchrotron radiation-based quasi-elastic scattering using time-domain interferometry with multi-line gamma rays, Sci. Rep. 7 (1) (2017) 1–9.

[36] F. Caporaletti, A.I. Chumakov, R. Rüffer, G. Monaco, Accessing the non-ergodicity factor of o-terphenyl via multi-line nuclear γ-resonance time-domain interferometry, Philos. Mag. 100 (20) (2020) 2646–2657.

[37] R. Rüffer, A.I. Chumakov, Nuclear resonance beamline at esrf, Hyperfine Interact. 97 (1) (1996) 589–604.

[38] F. Kremer, A. Loidl, The scaling of relaxation processes—revisited, in: The Scaling of Relaxation Processes, Springer, 2018, pp. 1–21.

[39] J. Wuttke, Laplace–Fourier transform of the stretched exponential function: analytic error bounds, double exponential transform, and open-source implementation "libkww", Algorithms 5 (4) (2012) 604–628.

[40] S. Mossa, G. Ruocco, M. Sampoli, Molecular dynamics simulation of the fragile glass former orthoterphenyl: a flexible molecule model. II. Collective dynamics, Phys. Rev. E 64 (2) (2001) 021511.

[41] F. Sciortino, L. Fabbian, S.-H. Chen, P. Tartaglia, Supercooled water and the kinetic glass transition. II. Collective dynamics, Phys. Rev. E 56 (5) (1997) 5397.

[42] A. Tölle, J. Wuttke, H. Schober, O. Randl, F. Fujara, Wavenumber dependence of structural relaxation in a molecular liquid, Eur. Phys. J. B, Condens. Matter Complex Syst. 5 (2) (1998) 231–236.

[43] B. Ruta, S. Hechler, N. Neuber, D. Orsi, L. Cristofolini, O. Gross, B. Bochtler, M. Frey, A. Kuball, S. Riegler, et al., Wave-vector dependence of the dynamics in supercooled metallic liquids, Phys. Rev. Lett. 125 (5) (2020) 055701.

[44] M. Oguni, J.-i. Sekine, H. Mine, Effects of the presence/absence of hydroxyl or amine groups in mono/di-substituted benzenes on the α and β structural relaxation properties in liquids and glasses, J. Non-Cryst. Solids 352 (42–49) (2006) 4665–4671.

[45] I. Artaki, J. Jonas, Nmr study of the dynamic structure of isopropylbenzene, Mol. Phys. 55 (4) (1985) 867–885.

[46] A.L. Plofker, P.A. Beckmann, Solid-state proton spin relaxation and methyl reorientation in isopropylbenzene, J. Phys. Chem. 99 (1) (1995) 391–394.

[47] K. Ngai, Microscopic understanding of the Johari-Goldstein β relaxation gained from nuclear γ-resonance time-domain-interferometry experiments, Phys. Rev. E 104 (1) (2021) 015103.

[48] Q. Yang, S. Wei, Y. Yu, H.-R. Zhang, L. Gao, Q.-Z. Bu, N. Amini, Y.-D. Cheng, F. Yang, A. Schökel, et al., Structural length-scale of β relaxation in metallic glass, J. Chem. Phys. (2022).

[49] C. Chakravarty, P.G. Debenedetti, F.H. Stillinger, Lindemann measures for the solid-liquid phase transition, J. Chem. Phys. 126 (20) (2007) 204508.

[50] K. Ngai, S. Capaccioli, P. Lunkenheimer, A. Loidl, Arriving at the most plausible interpretation of the dielectric spectra of glycerol with help from quasielastic γ-ray scattering time-domain interferometry, Phys. Rev. E 105 (5) (2022) 054609.

[51] K. Ngai, P. Lunkenheimer, C. Leon, U. Schneider, R. Brand, A. Loidl, Nature and properties of the Johari–Goldstein β-relaxation in the equilibrium liquid state of a class of glass-formers, J. Chem. Phys. 115 (3) (2001) 1405–1413.

[52] P. Lunkenheimer, A. Loidl, Dielectric spectroscopy of glass-forming materials: α-relaxation and excess wing, Chem. Phys. 284 (1–2) (2002) 205–219.

[53] C. Gainaru, R. Kahlau, E.A. Rössler, R. Böhmer, Evolution of excess wing and β-process in simple glass formers, J. Chem. Phys. 131 (18) (2009) 184510.

[54] J. Gabriel, F. Pabst, T. Blochowicz, Debye process and β-relaxation in 1-propanol probed by dielectric spectroscopy and depolarized dynamic light scattering, J. Phys. Chem. B 121 (37) (2017) 8847–8853.

[55] A. Döß, M. Paluch, H. Sillescu, G. Hinze, From strong to fragile glass formers: secondary relaxation in polyalcohols, Phys. Rev. Lett. 88 (9) (2002) 095701.

[56] A. Döß, M. Paluch, H. Sillescu, G. Hinze, Dynamics in supercooled polyalcohols: primary and secondary relaxation, J. Chem. Phys. 117 (14) (2002) 6582–6589.

[57] G. Johari, Source of JG-relaxation in the entropy of glass, J. Phys. Chem. B 123 (13) (2019) 3010–3023.

[58] T. Hikima, M. Hanaya, M. Oguni, Microscopic observation of a peculiar crystallization in the glass transition region and β-process as potentially controlling the growth rate in triphenylethylene, J. Mol. Struct. 479 (2–3) (1999) 245–250.

[59] T. Ichitsubo, E. Matsubara, T. Yamamoto, H. Chen, N. Nishiyama, J. Saida, K. Anazawa, Microstructure of fragile metallic glasses inferred from ultrasound-accelerated crystallization in pd-based metallic glasses, Phys. Rev. Lett. 95 (24) (2005) 245501.

[60] Z. Wang, B. Sun, H. Bai, W. Wang, Evolution of hidden localized flow during glass-to-liquid transition in metallic glass, Nat. Commun. 5 (1) (2014) 5823.

[61] Y. Duan, L. Zhang, J. Qiao, Y.-J. Wang, Y. Yang, T. Wada, H. Kato, J. Pelletier, E. Pineda, D. Crespo, Intrinsic correlation between the fraction of liquidlike zones and the β relaxation in high-entropy metallic glasses, Phys. Rev. Lett. 129 (17) (2022) 175501.

[62] F. Zhu, H. Nguyen, S. Song, D.P. Aji, A. Hirata, H. Wang, K. Nakajima, M. Chen, Intrinsic correlation between β-relaxation and spatial heterogeneity in a metallic glass, Nat. Commun. 7 (1) (2016) 11516.